Supporting Information

Efficient and robust intrinsically stretchable organic solar cells via mechanically interlocked oligomer integration

Xinrui Liu,[a] Xuanang Luo,[a] Jingchuan Chen,[a] Zhiyuan Yang,[a] Yingying Liu,[a] Ruixue Bai,*[b] Lei Ying,[a] Wenkai Zhong*[a]

[a] Institute of Polymer Optoelectronic Materials and Devices, Guangdong Basic Research Center of Excellence for Energy & Information Polymer Materials, State Key Laboratory of Luminescent Materials and Devices, South China University of Technology, Guangzhou 510640, China
E-mail: wkzhong@scut.edu.cn

[b] State Key Laboratory of Synergistic Chem-Bio Synthesis, Frontiers Science Center for Transformative Molecules, School of Chemistry and Chemical Engineering, Shanghai Jiao Tong University, Shanghai 200240, China
E-mail: rxbai0818@sjtu.edu.cn

Experimental Section

Materials

All reagents and chemicals were sourced from commercial suppliers (Aldrich, Alfa Aesar, and J&K) and used as received. PTzBI-oF was obtained from Dongguan VoltAmp Optoelectronics Technology Company, Ltd. PY-IT, NDI-Ph and PFNDI-F3N were procured from Solarmer Inc (China). Oligo[2]rotaxane was synthesized following the previously reported methodology.[1]

Fabrication of OSCs on rigid substrate

The devices were fabricated with the structure of ITO/PEDOT:PSS/active layer/NDI-Ph/Ag. Indium tin oxide (ITO) substrates underwent sequential ultrasonic cleaning in detergent, deionized water, and isopropyl alcohol. Following overnight drying at 70°C, the substrates were subjected to oxygen plasma treatment for 2 min. A ~20 nm-thick PEDOT:PSS layer (Clevios PVP Al 4083) was then deposited via spin-coating at 4000 rpm for 30 s, followed by thermal annealing at 150°C for 15 min. For the active layer preparation, PTzBI-oF:PY-IT (1:1.2, wt:wt) was dissolved in chloroform containing 25 mg/mL 2-ethoxynaphthalene (2-EN) at a total concentration of 7 mg/mL. To formulate ternary blends, oligo[2]rotaxane was first dissolved in chloroform (5 mg/mL) and subsequently mixed with the binary solution at designated ratios. All blend solutions were spin-coated at 2500 rpm onto the PEDOT:PSS layer, followed by thermal annealing at 100°C for 10 min in a nitrogen-filled glovebox. An interfacial layer was then introduced by spin-coating a 1.5 mg/mL NDI-Ph methanol solution at 3000 rpm. Finally, a 100 nm-thick Ag electrode was thermally evaporated through a shadow mask under high vacuum (3×10^{-7} Torr). The device active area was defined as 0.05 cm^2, with a metal aperture further restricting the effective area to 0.032 cm^2 for *J-V* curve characterizations.

Fabrication of IS-OSCs

IS-OSCs were prepared with structure of TPU/PEDOT:PSS (M-PH1000)/PEDOT:PSS

(4083)/active layer/PFNDI-F3N/EGaIn@Ag. The stretchable and transparent electrode (M-PH1000) was prepared by modifying PH1000 via the addition of 5 vol% dimethyl sulfoxide, 2 vol% polyethylene glycol, and 0.5 vol% FS-30. The formulated solution was spin-coated onto oxygen plasma-treated TPU substrates at 1200 rpm, followed by thermal annealing at 100℃ for 20 min. Next, PEDOT:PSS (4083) layer was spin-coated at 3000 rpm onto PH1000/TPU and annealed under at 100℃ for 20 min. Subsequently, the active layers were spin-coated under the same conditions used for rigid OSC fabrication. A solution of PFNDI-F3N (1 mg/mL in methanol) was then spin-coated at 3000 rpm on the active layers. A 100 nm-thick Ag electrode was thermally evaporated through a shadow mask under high vacuum (3×10^{-7} Torr). Finally, EGaIn liquid metal was sprayed onto the Ag layer through a deposition mask. The effective area of the as-prepared device was defined as 0.04 cm^2.

Theoretical calculations

The DFT calculation was carried out with the Gaussian 16 and Multiwfn software. The structure optimization for the oligo[2]rotaxane and the molecules was conducted on the basis of b3lyp-D3/6-31g**. The ESP was then calculated on the basis of b3lyp-D3/def-tzvp using the optimized structures. The dimer conformations are obtained with the forcite molecular dynamics. The dimer interaction was calculated based on b3lyp-D3/6-31+g** and illustrated with the Multiwfn and VMD software, with blue, green, and red color representing the PY-IT, oligo[2]rotaxane, and PTzBI-oF, respectively.

The ring moves under tensile simulation was investigated using the forcite with the optimized structures going by the following procedures: (1) an amorphous cell with four oligo[2]rotaxane chains (initial density = 0.5 g cm^{-3}) was built using the structures from the DFT calculation. (2) 5 annealing cycles from 300 to 1000 K (NPT) were conducted to obtain random distributions. (3) The cell was subjected to successive dynamics of 500 ps molecular dynamics (NVT, T = 300 K) to obtain the stable conformation. (4) The cell was then subjected to a stress-strain script with stress successive increased to 2.5 GPa, obtaining the stress-strain relationship. The final

structures are demonstrated in Fig. 1b.

OSC Device characterizations

The *J-V* curves were measured using a Keithley 2400 source meter under illumination (100 mW cm^{-2}) provided by an AM 1.5G solar simulator (SS-F5-3A, Enlitech) within a nitrogen-filled glovebox. EQE spectra were measured using an EQE measurement system (QE-R3011, Enlitech), with the light intensity at each wavelength calibrated using a standard single-crystal Si solar cell. EQE_{EL} measurements were performed by applying external voltage/current sources through the devices (ELCT-3010, Enlitech). Capacitance-Voltage (*C-V*), Capacitance-Frequency (*C-ω*), and photo-induced charge extraction by linearly increasing voltage (Photo-CELIV) measurements were conducted using the PAIOS platform (Fluxim), which integrates characterization capabilities for both solar cells and organic light-emitting diodes (OLEDs).

The energetic profile of trap density of states (tDOS) can be derived from the angular frequency dependent capacitance using the equation:

$$N_T\left(E_\omega\right) = -\frac{V_{bi}}{qW}\cdot\frac{dC}{d\omega}\cdot\frac{\omega}{kT}$$

where ω is the angular frequency, C is the capacitance, q is the elementary charge, k is the Boltzmann's constant and T is absolute temperature. V_{bi} and W are the built-in potential and depletion width, respectively, which were extracted from the Mott-Schottky analysis. The applied angular frequency ω defines an energetic demarcation.

$$E_\omega = kT\ln\left(\frac{\omega_0}{\omega}\right)$$

where ω_0 is the attempt-to-escape frequency. The trap states below the energy demarcation can capture or emit charges with the given ω and contribute to the capacitance.

General characterizations

Stress-strain curves: The tensile tests were performed through the following steps: (1)

the thin film was prepared onto a PEDOT:PSS-coated ITO glass substrate and post-treated with conditions identical to device fabrication; (2) the resultant sample was floated on deionized water, with the hydrophilic PEDOT:PSS layer dissolved within 5 min, leaving a freestanding hydrophobic active layer film at the air-water interface; (3) a tensile testing stage equipped with frosted aluminum grips was positioned to adhere the floating film via van der Waals interactions; (4) gradual water removal allowed the film to self-align under interfacial tension, leaving a free-standing active layer film on the tensile stage. Uniaxial stretching was performed at a constant crosshead speed of 0.01 mm/min. Engineering stress (σ) and strain (ε) were calculated as:

$$Stress = F / (A \times B)$$

$$Strain = \Delta l / l_0$$

where F is the applied force recorded by a high-sensitive force sensor, A is the width of films, B is the thickness of the films, Δl is the elongation of the film, and l_0 is the initial distance between the clamps.

Film-on-elastomer (FOE) method: FOE tests were done by an optical microscope (MJ31, Mshot) and a custom-designed tensile stage. The films were coated on glasses (size: 1.5 cm ×1.5 cm) and then transferred to the PDMS film. The PDMS was stretched until crack evolution in the film was observed under the optical microscope.

UV-vis-NIR absorption spectra: The UV-vis-NIR absorption spectra of the thin films were measured using a SHIMADZU UV-3600 spectrophotometer. The films were prepared by spin-coating a 7 mg/mL solution onto quartz substrates. All samples for absorption characterization were prepared with same conditions for device fabrication.

Differential Scanning Calorimetry (DSC): DSC measurements were conducted under a nitrogen atmosphere using a DSC 200 F3 calorimeter (NETZSCH Scientific Instruments). For pristine polymers, the temperature range was set from 0 to 300 °C, while for polymer/oligo[2]rotaxane blend films, the range was from 0 to 120 °C. All

measurements were performed with a heating/cooling rate of 10 °C min^{-1}.

XPS measurement: X-ray photoelectron pectroscopy (XPS) were determined by British Kratos X-ray photoelectron spectroscopy for element analysis. The films were spin-coated on ITO substrates.

Time-resolved photoluminescence (TRPL): TRPL measurements were performed on a Horiba Fluorolog-3 system equipped with a Time-Correlated Single Photon Counting system. The neat PTzBI-oF film were excited by 450 nm laser and detected at its PL emission peak (~740 nm). The neat PY-IT, PTzBI-oF:PY-IT, and PTzBI-oF:PY-IT: oligo[2]rotaxane blends were excited by 450 nm laser and detected at 825 nm.

Transient absorption (TA) spectroscopy: The seed light has a wavelength of 700 nm, with a single pulse energy reaching 2 mJ and a repetition rate of 500 Hz. This seed light is split into two beams: the stronger one generates a white light continuum with approximately 100 μW, serving as the probe light. The pulse duration is around 150 fs, and the pump light can pass through a chopper to reduce the repetition rate to 250 Hz. TA spectra were obtained by comparing the probe light spectra with and without pump light excitation. The chirp dispersion of the probe light was numerically corrected during data processing, with the delay time for different wavelengths fitting the Cauchy empirical formula[2].

Nano infrared spectroscopy atomic force microscopy (AFM-IR): AFM-IR was performed by Anasys nanoIR3 (Bruker).

Grazing incidence wide angle scattering (GIWAXS): GIWAXS measurements were performed on the Bruker D8 Venture instrument. The films were spin-coated on PEDOT:PSS/silicon wafers (1.5 cm × 1.5 cm) under processing conditions same to those used for device fabrication. The X-ray energy was set to 9.24 keV. The incident angle of the X-ray was set to 0.20°. The sample-to-detector distance was about 70 mm.

Scattering signals were collected using a CCD detector with a pixel size of 0.135 mm × 0.135 mm. Data reduction and analysis were performed using the Igor-based Nika package.[3]

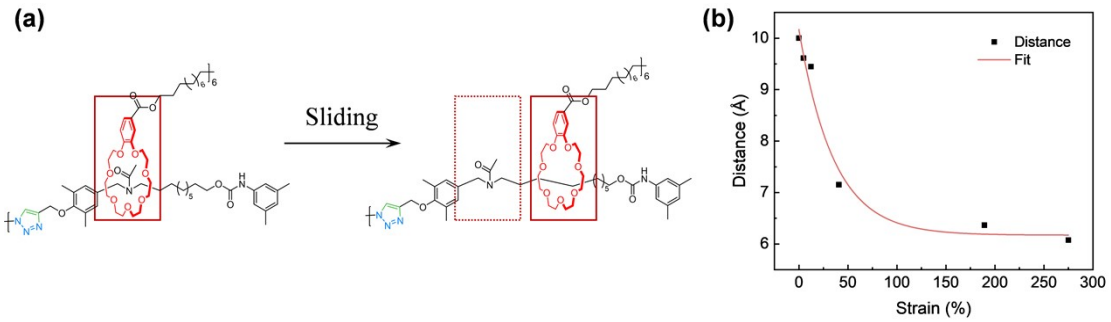

Fig. S1 (a) Schematic illustration of the directional sliding motion of the macrocycle along the axle in oligo[2]rotaxane; (b) Distance variation between the macrocycle and the urethane moiety along the axle chain during uniaxial stretching, as revealed by MD simulations.

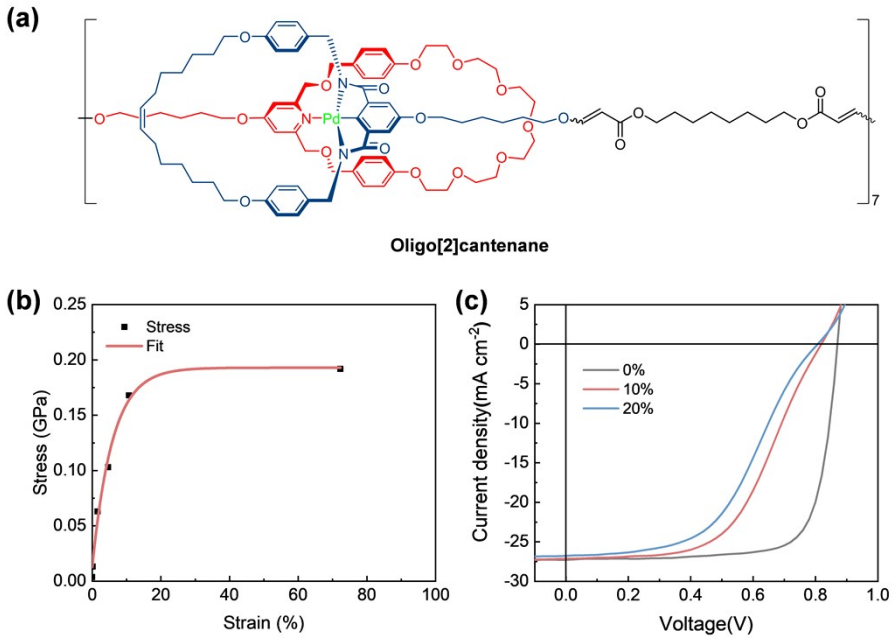

Fig. S2 (a) Chemical structures of oligo[2]cantenane. (b) MD-simulated σ-ε curve for oligo[2]cantenane amorphous aggregates under stretching. (c) *J-V* curves of PTzBI-oF:PY-IT:oligo[2]cantenane OSC devices, with oligo[2]cantenane weight ratios of 0%, 10%, and 20% relative to PTzBI-oF.

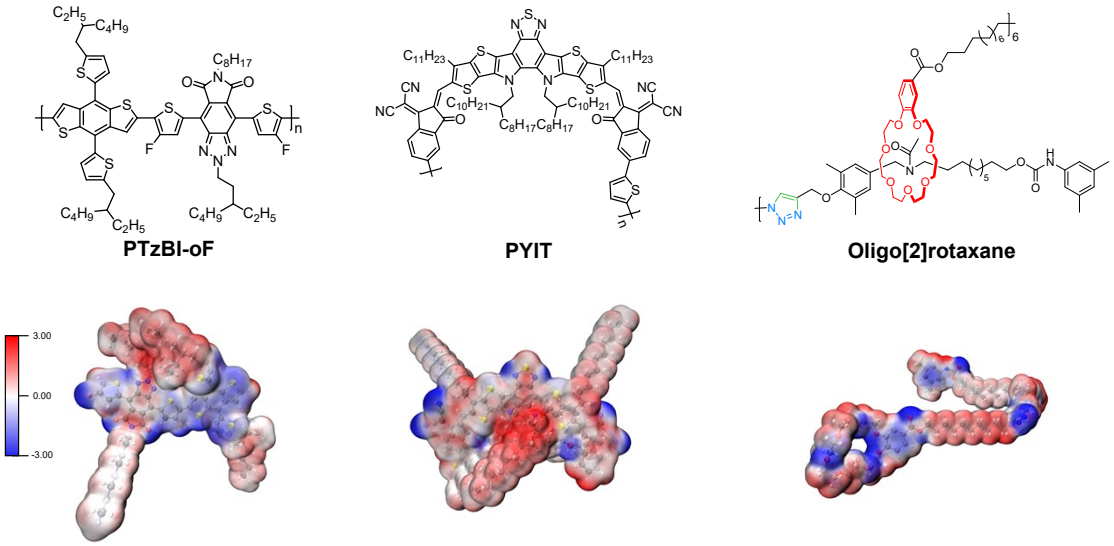

Fig. S3 ESP distributions of PTzBI-oF, PY-IT and oligo[2]rotaxane.

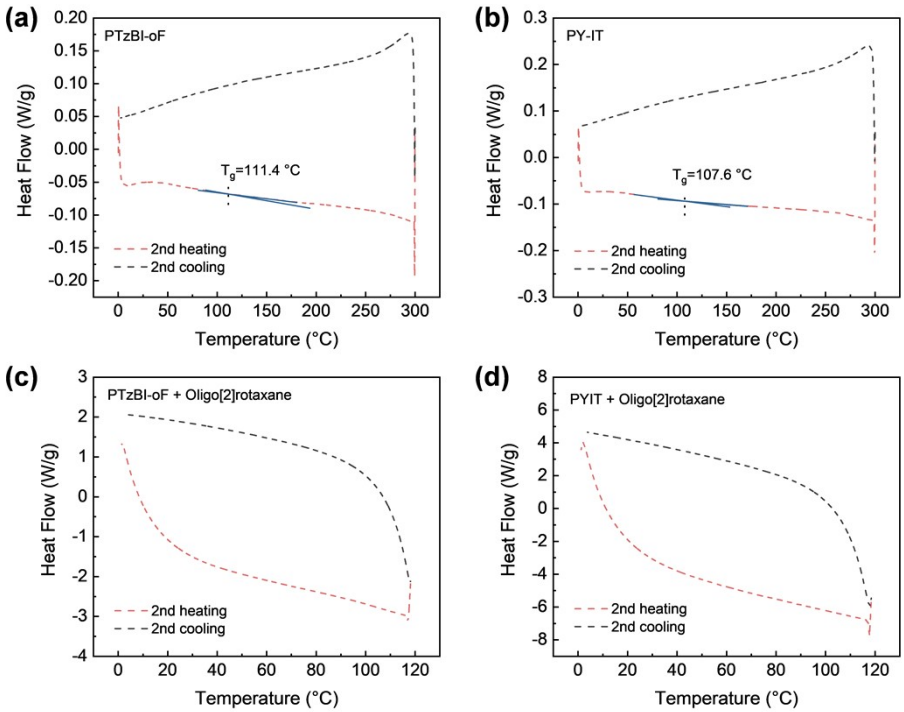

Fig. S4 DSC curves of (a) PTzBI-oF, (b) PY-IT, (c) PTzBI/oligo[2]rotaxane, and (d) PY-IT/oligo[2]rotaxane. The oligo[2]rotaxane in mixtures is at 10% weight ratio relative to the polymer.

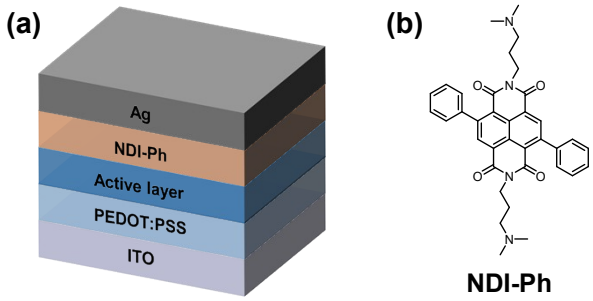

Fig. S5 (a) OSC Device structure used in this work. (b) Chemical structures of NDI-Ph.[4]

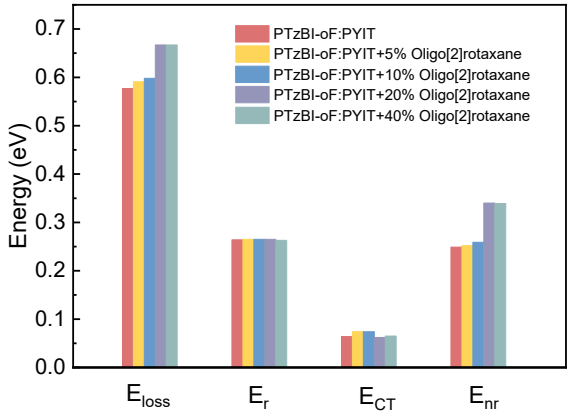

Fig. S6 Energy loss mapping of OSC devices based on PTzBI-oF:PY-IT: oligo[2]rotaxane blend films.

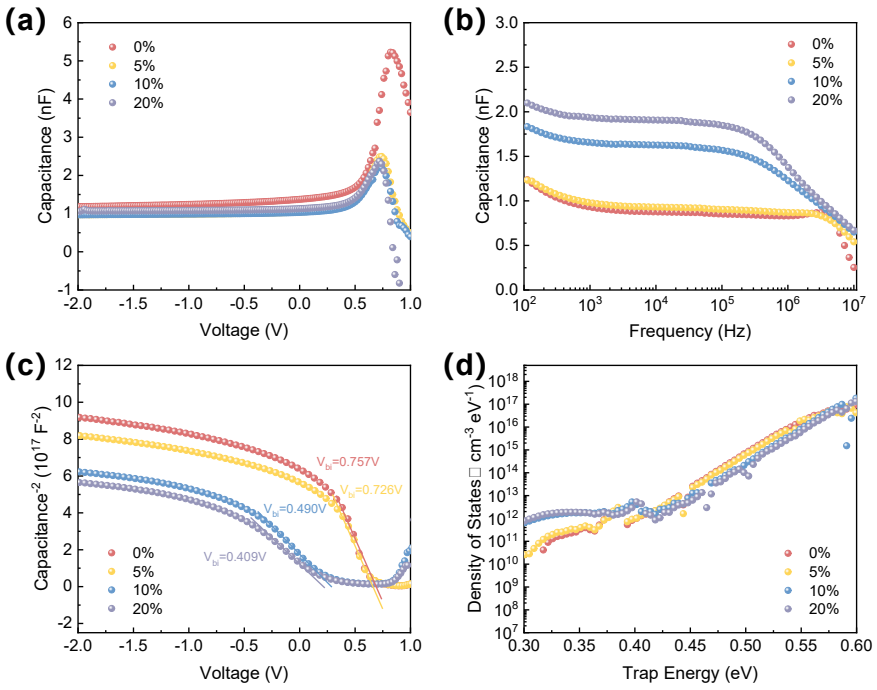

Fig. S7 (a) *C-V* curves, (b) *C-F* characteristics, (c) Mott-Schottky plots, and (d) trap density of states (tDOS) for OSC devices based on PTzBI-oF:PY-IT:oligo[2]rotaxane blend films.

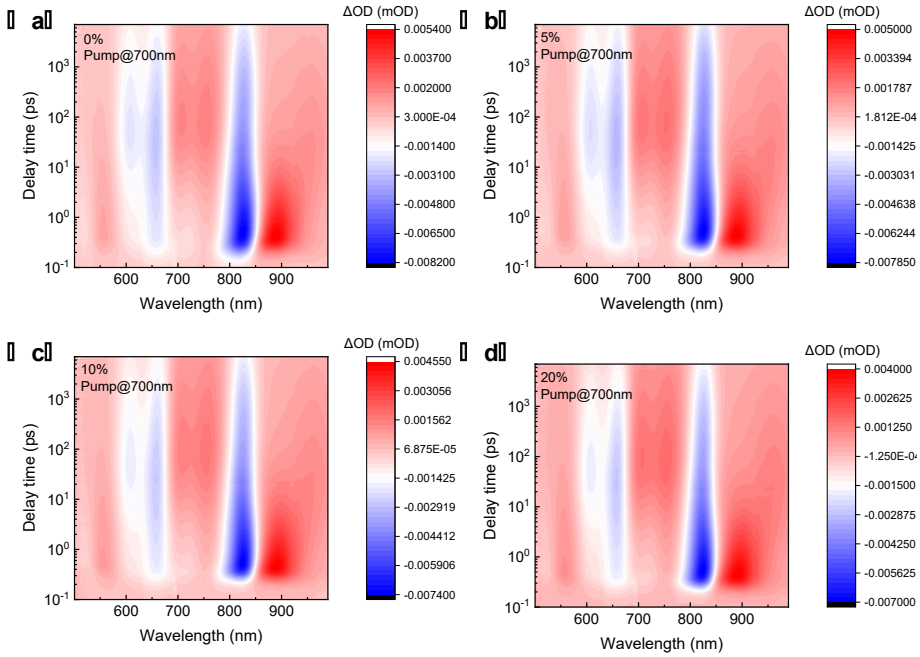

Fig. S8 2D contour images of TA spectra for PTzBI-oF:PY-IT:oligo[2]rotaxane blend films with varying oligo[2]rotaxane contents.

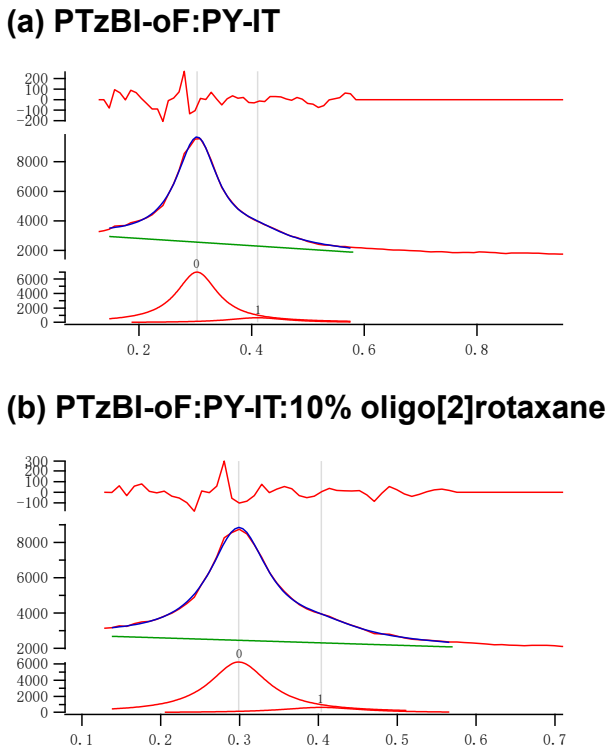

Fig. S9 Fitting details (peak 0: Lorentz; peak 1: Lorentz) for the lamellar and $(11\bar{1})$ reflections of the I-q curves in the IP direction: (a) PTzBI-oF:PY-IT; (b) PTzBI-oF:PY-IT:10% oligo[2]rotaxane.

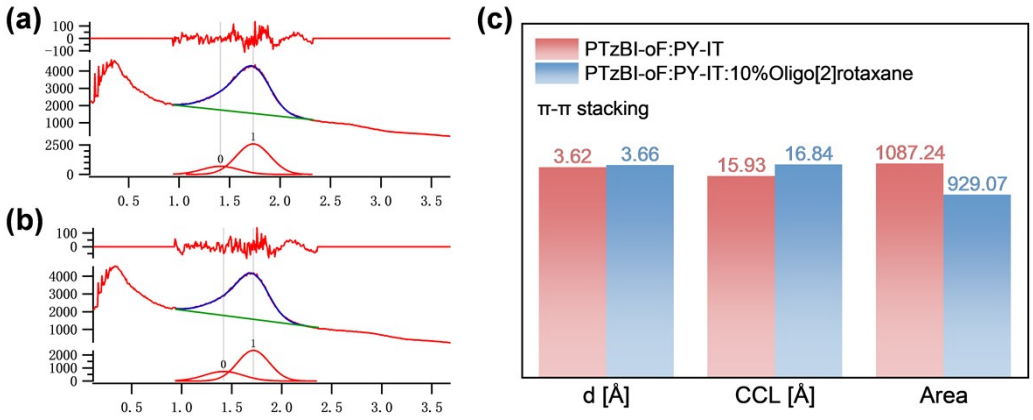

Fig. S10 Illustration of the multi-peak fit to the π-π stacking in the OOP direction, with two Gauss functions: (a) PTzBI-oF:PY-IT; (b) PTzBI-oF:PY-IT:10% oligo[2]rotaxane blend films. (b) Summary of d-spacing, CCL, and peak area of the π-π stacking.

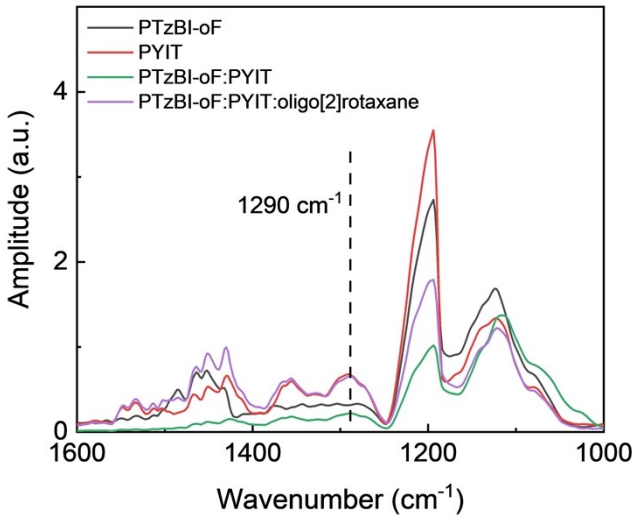

Fig. S11 IR spectra of pristine PTzBI-oF, PY-IT, oligo[2]rotaxane, and their blend films.

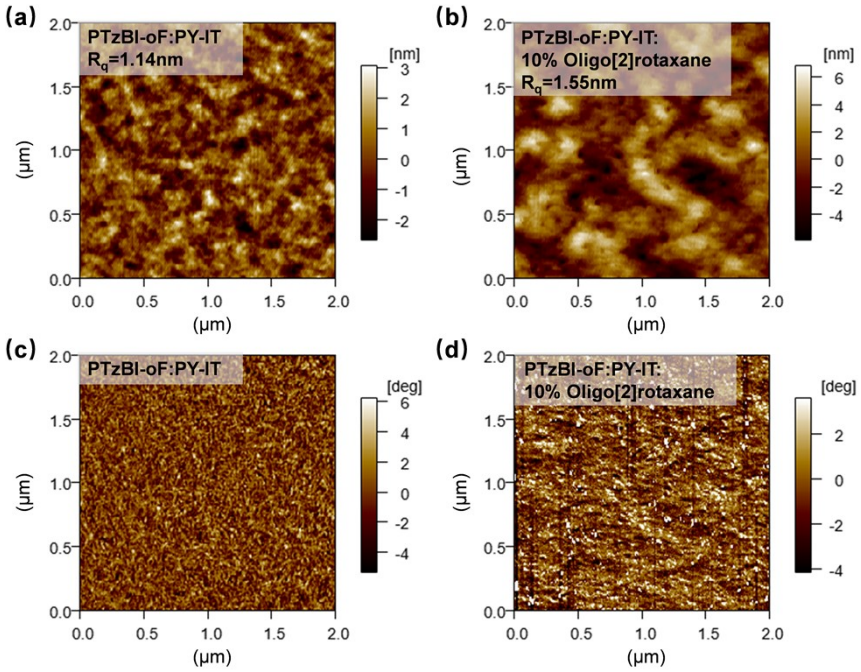

Fig. S12 AFM (a) height images and (b) phase images of PTzBI-oF:PY-IT and PTzBI-oF:PY-IT:10% oligo[2]rotaxane blend films.

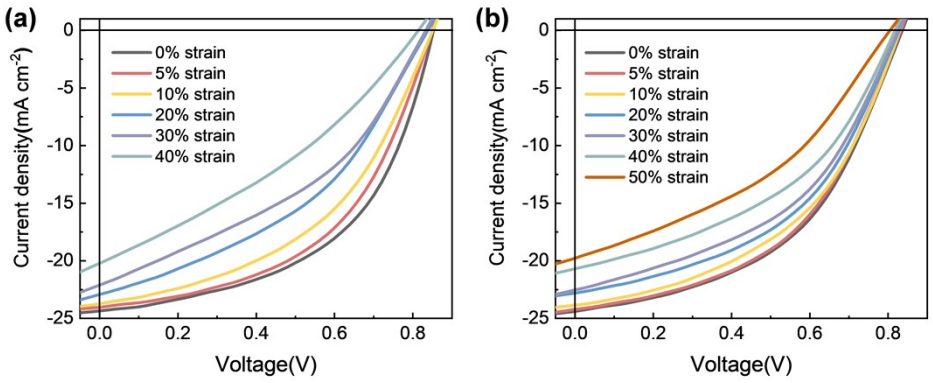

Fig. S13 *J-V* curves of IS-OSC devices based on (a) PTzBI-oF:PY-IT and (b) PTzBI-oF:PY-IT:10% oligo[2]rotaxane blend films under various strains.

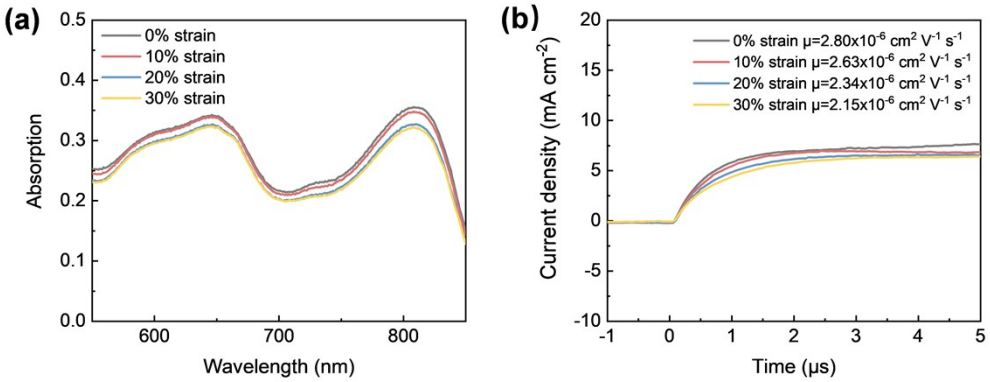

Fig. S14 (a) *In situ* UV-vis-NIR absorption spectra of the PTzBI-oF:PY-IT:10% oligo[2]rotaxane thin film during stretching. (b) Photo-CELIV curves of the PTzBI-oF:PY-IT:10% oligo[2]rotaxane IS-OSC devices upon various applied strains.

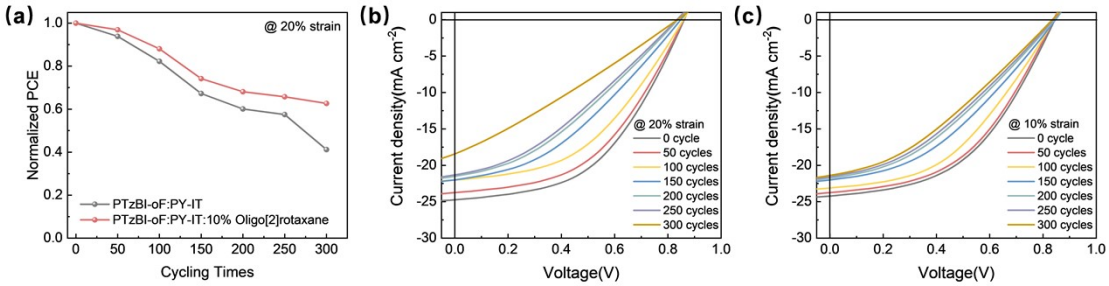

Fig. S15 (a) Normalized PCEs and (b,c) *J-V* curves of IS-OSCs subjected to 300 cycles of 20% uniaxial strain.

Table S1. Photovoltaic parameters of the PTzBI-oF:PY-IT:Oligo[2]cantenane based OSC devices, with oligo[2]cantenane weight ratios of 0%, 10%, and 20% relative to PTzBI-oF.

oligo[2]cantenane content	V_{OC} (V)	J_{SC} (mA cm^{-2})	FF (%)	PCE (%)
0%	0.870	27.26	76.16	18.07
10%	0.819	27.13	54.49	12.10
20%	0.807	26.77	49.63	10.72

Table S2. Energy loss parameters.

Oligo[2]rotaxane ratio	E_{loss} (eV)	E_r (eV)	E_{CT} (eV)	E_{nr} (eV)
0%	0.577	0.264	0.064	0.249
5%	0.591	0.265	0.074	0.252
10%	0.598	0.265	0.074	0.259
20%	0.667	0.265	0.062	0.340
40%	0.667	0.263	0.065	0.339

Table S3. The Gaussian fitting of the defect state density distribution curve and related parameters.

Oligo[2]rotaxane ratio	Peak type	Location（E_t）(eV)	Width (σ)
0%	Gauss	0.384	0.00989
5%	Gauss	0.384	0.01085
10%	Gauss	0.398	0.00982
20%	Gauss	0.403	0.00987

Table S4. Fitting results of TRPL of blend films.

	Excitation wavelength(nm)	Detection wavelength(nm)	τ (ns)
PTzBI-oF	450	825	0.567
PTzBI-oF:PY-IT			0.179
PTzBI-oF:PY-IT+5%Oligo[2]rotaxane			0.178
PTzBI-oF:PY-IT+10%Oligo[2]rotaxane			0.176
PTzBI-oF:PY-IT+20%Oligo[2]rotaxane			0.173

Table S5. Photovoltaic parameters of the PTzBI-oF:PY-IT IS-OSCs under different strains.

Strain	V_{OC} (V)	J_{SC} (mA cm^{-2})	FF (%)	PCE (%)
0%	0.853	24.35	52.13	10.82
5%	0.850	24.04	50.39	10.29
10%	0.851	23.73	46.33	9.35
20%	0.838	22.92	41.36	7.94
30%	0.833	22.11	39.13	7.21
40%	0.814	20.22	33.31	5.48

Table S6. Photovoltaic parameters of the PTzBI-oF:PY-IT:10% oligo[2]rotaxane based IS-OSCs under different strains.

Strain	V_{OC} (V)	J_{SC} (mA cm^{-2})	FF (%)	PCE (%)
0%	0.836	24.39	48.61	9.91
5%	0.833	24.21	48.32	9.74
10%	0.829	23.85	47.10	9.32
20%	0.828	22.80	46.91	8.86
30%	0.825	22.52	45.22	8.41
40%	0.818	20.69	43.59	7.37
50%	0.805	19.78	39.03	6.21

Table S7. Photovoltaic parameters of the PTzBI-oF:PY-IT based IS-OSCs subjected to 300 cycles of 20% uniaxial strain.

Cycles	V_{OC} (V)	J_{SC} (mA cm^{-2})	FF (%)	PCE (%)
0	0.861	24.74	48.90	10.42
50	0.859	23.75	47.96	9.78
100	0.858	22.01	45.40	8.57
150	0.848	22.01	37.55	7.01
200	0.837	21.51	34.75	6.26
250	0.833	21.32	33.72	5.99
300	0.835	18.43	27.85	4.29

Table S8. Photovoltaic parameters of the PTzBI-oF:PY-IT:oligo[2]rotaxane based IS-OSCs subjected to 300 cycles of 20% uniaxial strain. The weight ratio of oligo[2]rotaxane was at 10% relative to PTzBI-oF.

Cycles	V_{OC} (V)	J_{SC} (mA cm^{-2})	FF (%)	PCE (%)
0	0.845	24.23	47.49	9.72
50	0.840	23.74	47.24	9.42
100	0.841	23.12	44.03	8.56
150	0.847	22.01	38.67	7.21
200	0.843	21.74	36.12	6.62
250	0.839	21.59	35.24	6.39
300	0.835	21.39	34.08	6.09

References

1 R. Bai, W. Wang, W. Gao, M. Yang, X. Zhang, C. Wang, Z. Fan, L. Yang, Z. Zhang, X. Yan, *Angew. Chem. Int. Ed.,* 2024, **63**, e202410127.

2 K. Chen, A. Barker, J. Sutton, K. Prasad, J. Zhu, J. Zhou, K. Gordon, Z. Xie, X. Zhan, and J. M. Hodgkiss, *J. Am. Chem. Soc.*, 2019, **141**, 6922-6929.

3 J. Ilavsky, J. Appl, *Crystallogr*., 2012, **45**, 324-328.

4 Y. Yu, J. Wang, Y. Cui, Z. Chen, T. Zhang, Y. Xiao, W. Wang, J. Wang, X.-T. Hao, J. Hou, *J. Am. Chem. Soc.*, 2024, **146**, 8697-8705.